Two-dimensional seismic imaging of the Valhall model from synthetic OBC data by frequency-domain elastic full-waveform inversion

Romain Brossier [*], *Stéphane Operto* [*] *and Jean Virieux* [†]
[*] *Géoazur - Université Nice Sophia-Antipolis - CNRS ,* [†] *Laboratoire de Géophysique Interne et Tectonophysique, Université Joseph Fourier*

SUMMARY

Quantitative imaging of the elastic properties of the subsurface is essential for reservoir characterization. We apply two-dimensional frequency-domain full-waveform inversion (FWI) to image shallow-water synthetic V_P and V_S models of the Valhall oil and gas field from 3-C ocean-bottom-cable data. In soft-seabed environment where a small amount of P-to-S mode conversion occurs at the sea bottom, the seismic wavefield is dominated by the P waves whereas the S waves have a weaker signature. We first show that acoustic FWI of elastic data provides accurate V_P model in such environment. Elastic FWI, that is desired for reservoir characterization, is a more difficult task. Hierarchical processing of the different parameter classes and data components is required, in addition to low-frequency data and robust multi-scale algorithm, to converge toward acceptable models.

INTRODUCTION

Quantitative seismic imaging of earth parameters is one of the main challenge for reservoir characterization. Frequency-domain full-waveform inversion (FWI) allows to build accurate models of complex structures from wide-aperture acquisition geometries (Pratt and Worthington, 1990). Most of the applications of FWI to real data at different exploration scales were performed under the acoustic approximation (Ravaut et al., 2004; Operto et al., 2006; Bleibinhaus et al., 2007) while only few papers recently tackled the elastic problem (Shi et al., 2007). Elastic parameters reconstruction is indeed a difficult and highly non-linear problem. The initial model building, that directly drives the convergence of the inversion, is a difficult issue for the S-wave velocity parameter (or linked parameters such as the Poisson's ratio): indeed, imaging of the V_S parameter has potentially a high-resolution power due to the short S wavelengths, that makes the inversion more sensitive to the inacurracies of the starting model (Brossier et al., 2009). Free-surface effects, such as surface-waves and free-surface multiples, add additional non linearities in the inversion of land data, that require different hierarchical inversion regularizations (Gelis et al., 2007; Brossier et al., 2009). Weak P-to-S conversions in marine data with low S-wave velocity contrasts at the sea bed require the hierarchical reconstruction of the different parameter classes, and the hierarchical inversions of the different data components including careful phase selections for proper inversion convergence, even for simple canonical models (Sears et al., 2008). However, reconstruction of elastic parameters is useful in reservoir characterization: for example, Poisson's ratio anomalies are good marker of gas because the V_S is weakly affected by the presence of gas unlike the V_P one.

In this study, we present an application of frequency-domain elastic FWI to the synthetic Valhall model, representative of oil and gas fields in shallow water environment of North Sea. After a short review of elastic wave modeling and FWI, we first show that acoustic FWI of elastic data provided reliable V_P model in the Valhall geological environment. Second, we propose a multi-step strategy for elastic FWI, that allowed reliable reconstruction of V_S parameter in addition to that of the V_P model.

METHOD

Forward problem

Two-dimensional frequency-domain elastic FWI requires the solution of the two-way wave equation for P-SV waves in 2D heterogeneous media. We shall limit ourselves to the isotropic case in this study. In the frequency domain, one may write the elastic wave equation as:

$$\begin{aligned} -\imath\omega\rho\mathbf{V} &= \nabla\cdot\sigma+\rho f \\ -\imath\omega\sigma &= \mathbf{c}\colon\nabla\mathbf{V}-i\omega\sigma_0, \end{aligned} \qquad (1)$$

where unknown quantities of the forward problem are horizontal and vertical particle velocities $\mathbf{V}=(V_X,V_Z)$ and stress σ fields. The system 1 is discretized with a Discontinuous Galerkin method (Brossier et al., 2008). Low-order P_0 and P_1 interpolations are used for wavefield parameterization (figure 1). The P_1 interpolation is used on top of the model (in the first 160 meters) in an unstructured triangular mesh. This allows the accurate positioning of the sources and receivers in the mesh, by mean of the linear interpolation basis functions and the locally-refined mesh. The water-solid interface at a depth of 70 m is embedded inside the P_1 zone, because the P_0 interpolation is unstable at the water-solid interface (Brossier et al., 2008). For time and memory computational savings, the P_1 interpolation order is limited to the shallow part of the model, whereas the P_0 interpolation is used below 160 m on a regular equilateral mesh. The sparse linear system resulting from the discretization of system 1 is solved efficiently for multiple sources using the parallel direct solver MUMPS (Amestoy et al., 2006).

Inverse problem

Frequency-domain FWI (Pratt et al., 1998) is an optimization problem, which can be recast as a linearized least-squares problem that minimizes the misfit between the frequency-domain recorded data (d_{obs}) and modeled data ($d_{calc}^{(k)}$) at iteration k, defined by the objective function:

$$\mathscr{C}^{(k)}=\frac{1}{2}(d_{obs}-d_{calc}^{(k)})^{\dagger}\mathbf{S}_d{}^{\dagger}\mathbf{S}_d(d_{obs}-d_{calc}^{(k)}). \qquad (2)$$

Superscript † indicates the adjoint (transposed conjugate) and $\mathbf{S}_d$ is a diagonal weighting matrix applied to the misfit vector to scale the relative contributions of each of its components. The

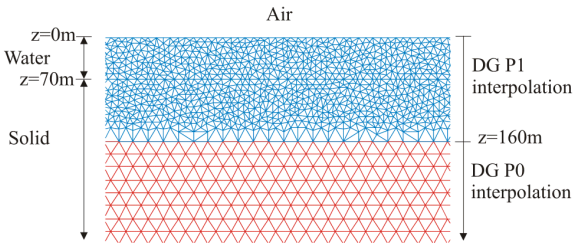

Figure 1: Close-up of the triangular mesh centred on the sea bottom, used for elastic wave propagation modeling in the Valhall model. P_1 and P_0 cells are displayed respectively in blue and red.

gradient $\mathscr{G}^{(k)}$ of the objective function is efficiently computed by the adjoint-state technique (Plessix, 2006), which requires solving only two forward problems per shot.

A second-order Taylor expansion of the objective function allows to find the Newton update $\delta\mathbf{m}$ which minimizes the objective function:

$$\mathbf{B}^{(k)}\delta\mathbf{m} = -\mathscr{G}^{(\mathbf{k})}, \tag{3}$$

where $\mathbf{B}^{(k)}$ is the Hessian matrix. Because of the huge computational time required to build $\mathbf{B}^{(k)}$, Newton method are generally avoided. Steepest Descent or Conjugate Gradient methods scaled by the diagonal terms of an approximate Hessian are generally used in FWI (Pratt et al., 1998; Operto et al., 2006; Shin et al., 2001). In this study, we use the Quasi-Newton L-BFGS method (Nocedal, 1980). L-BFGS provides an approximate inverse Hessian at a marginal computational extra cost, that is useful to improve the convergence rate of the iterative imaging process (Brossier et al., 2009).

Data preconditioning

Non-linearity of FWI can be efficiently mitigated by selecting a subset of specific arrivals (e.g., Sears et al., 2008). Data preconditioning can be applied in the frequency domain by means of complex frequencies $(\omega+\imath\gamma)$, which is equivalent to damp seismograms in time (Brenders and Pratt, 2007). The Fourier transform of a signal $f(t)$ damped in time by $exp^{-\gamma(t-t_0)}$ is given by:

$$F(\omega+\imath\gamma)exp^{\gamma t_0} = \int_{-\infty}^{+\infty} f(t)exp^{-\gamma(t-t_0)}exp^{-\imath\omega t}dt, \tag{4}$$

where the damping, controlled by the γ parameter, can be applied from an arbitrarily arrival time t_0, which usually corresponds to the first-arrival time. Time-damping applied from the first-arrival time can be viewed as a heuristic way to select aperture angles in the data. This aperture selection can be exploited to implement a second-level of hierarchy in the multi-scale inversion, in addition to that provided by the frequency selection: during each successive frequency inversion, we hierarchically performed several inversion iterations using decreasing imaginary terms γ to progressively inject in the inversion more resolving arrivals associated with later-arriving phases (i.e., shorter-aperture phases). This strategy revealed useful for inversion of land data (Brossier et al., 2009) and will be used in this study.

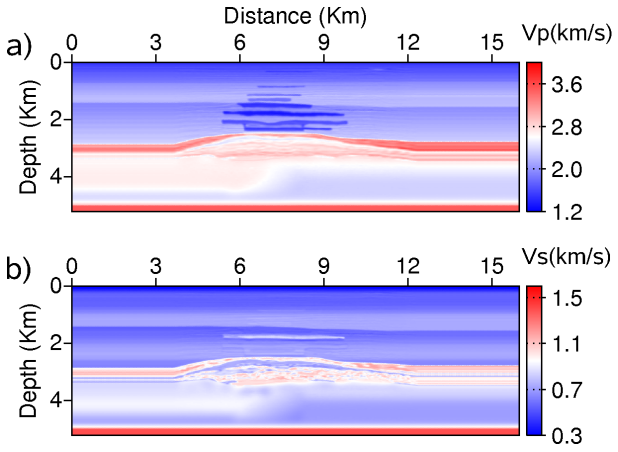

Figure 2: Synthetic Valhall models. a) V_P, b) V_S.

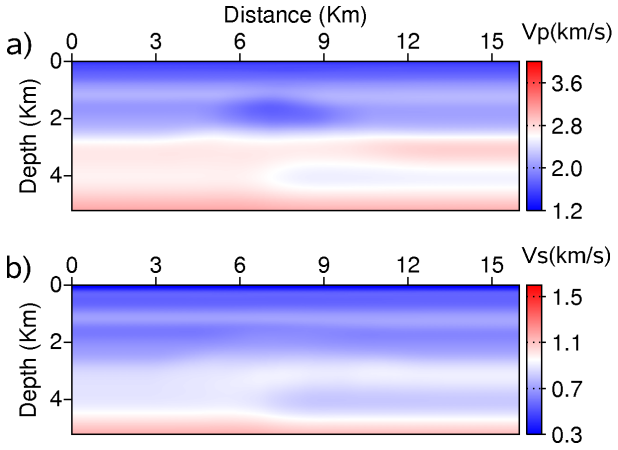

Figure 3: Initial V_P (a) and V_S (b) models for FWI.

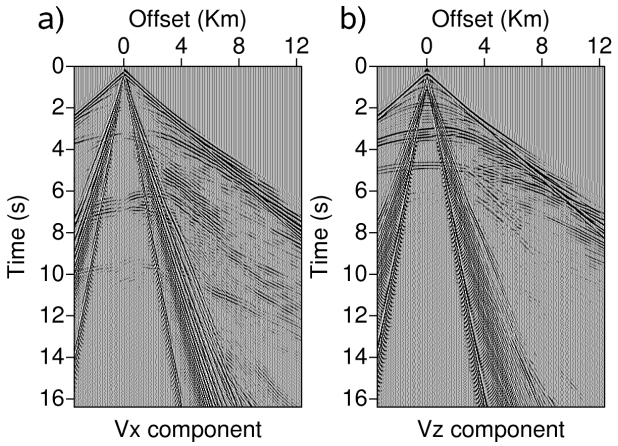

Figure 4: Example of time-domain shot gather for a source at $x = 3\,km$ in the synthetic Valhall elastic models for a) horizontal component and b) vertical one of geophones.

VALHALL ELASTIC MODEL AND DATA

The figure 2 shows the V_P and V_S synthetic models provided by BP. The main targets are the gas cloud in the large sediments layer, and the trapped oil underneath the cap rock composed of chalk in a deeper part of the model. Gas clouds are easily identified by the low P-wave velocities, whereas their signature is

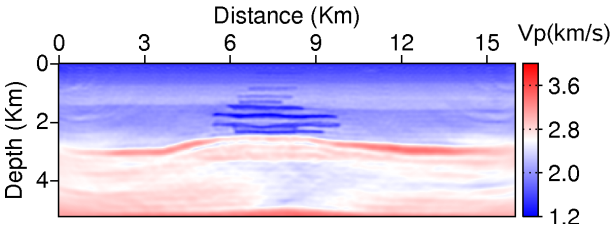

Figure 5: V_P model inferred from acoustic FWI of elastic data.

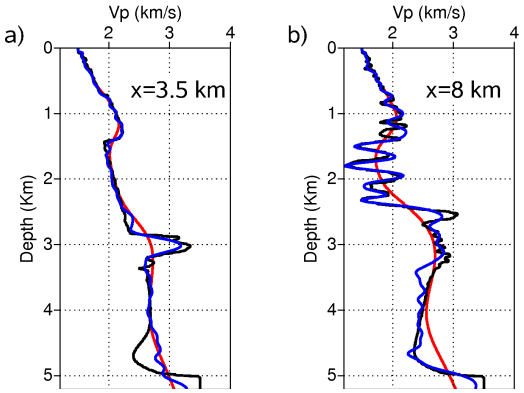

Figure 6: Vertical logs at distances a) 3.5 km and b) 8 km extracted from the FWI model of Figure 5. True, starting and FWI models are displayed in black, red and blue, respectively.

much weaker in the V_S model. In this study, density is considered constant and assumed to be known during the inversion. Starting models (Figure 3) are inferred from the true ones by Gaussian smoothing, the vertical correlation of which linearly increases from 25 m at the water-solid interface to 1000 m at 5200 m depth. The horizontal correlation length is 500 m.

The acquisition geometry mimics an OBC acquisition. 315 pressure sources are located 6 m below the water surface with an horizontal spacing of 50 m. 315 3-C sensors spaced by 50 m, each composed of one hydrophone, and one vertical and inline horizontal geophones, are located at a depth of 70 m on the sea bottom.

A time-domain shot-gather is shown in figure 4 for the V_X and the V_Z components. Low V_S on the sea bottom and the relatively smooth V_S model led to small-amplitude converted P-to-S waves on both the vertical and horizontal components, and made the reconstruction of the V_S model ill-posed.

In this study, the elastic observed data have been computed with the frequency-domain P_0-P_1 DG method for the frequencies and damping factors used in inversion. The maximum frequency involved in the inversion was 6 Hz, and the triangular mesh was designed according to the minimum S wavelength at this frequency (Figure 1). For all the tests, source signature is estimated by linear inversion during each frequency inversion iteration (Pratt, 1999).

ACOUSTIC INVERSION OF ELASTIC DATA

We should consider first acoustic FWI of elastic data. As observed in the figure 4, P arrivals dominate the seismic wavefield (especially, on the vertical geophone and hydrophone), leading to a favorable framework for acoustic FWI (Barnes and Charara, 2008).

Acoustic FWI was performed with the FWT2D code (Sourbier et al., 2009) based on a finite-difference forward problem engine to solve the Helmholtz equation. Five frequencies were inverted successively (2, 3, 4, 5 and 6 Hz) using 3 damping factors ($\gamma = 2, 0.33, 0.1$) applied in cascade during each frequency inversion. The inversion was applied to the hydrophone component. The initial V_P model for acoustic FWI is shown in figure 3a. The steepest Descent method was used for optimization, preconditioned by the diagonal terms of the approximate Hessian (Operto et al., 2006). Fifteen iterations were performed per damping factor leading to 45 iterations per frequency inversion. The final FWI V_P model does not exhibit significant artifacts (Figure 5). Comparison between V_P logs, extracted from the true and final FWI models, shows a reliable reconstruction of the P-wave velocities, in spite of the low frequencies involved in the inversion (Figure 6).

These results suggest that acoustic FWI can be relevant in some marine case studies, where elastic effects have a relatively-weak signature in the data. The resulting V_P model may be used as a starting model to proceed with elastic FWI in later stage.

ELASTIC FULL-WAVEFORM INVERSION

Inversion set-up

We now applied elastic FWI to the 3-C OBC data. Sears et al. (2008) have illustrated that elastic FWI is ill-posed when the S-wave velocity models exhibit relatively small contrasts, that prevent recording of significant P-to-S converted waves. In order to mitigate the ill-posedness of FWI, they designed a multi-step strategy, that was adapted to the frequency-domain FWI as described below:

1- In a first step, V_P is reconstructed from the hydrophone data. The forward problem is performed with the elastic DG method but the V_S model is left unchanged during FWI. The aim of this first stage is to improve the V_P model to significantly decrease the P-wave residuals. During this first step, a coarse mesh adapted to the V_P wavelength was designed for computational efficiency. In this case, S-wave modeling was affected by numerical dispersion, that, however, did not significantly impact the V_P-model reconstruction. Note that the final V_P model of this first stage is close to that of acoustic inversion.

2- In a second step, the V_P and V_S models are reconstructed simultaneously from the horizontal and vertical components of geophones. A gain, given by the source-receiver offset to the power of 2, was applied to the data through the matrix $\mathbf{S}_d$. The aim of this weighting was to increase the weight of the intermediate-to-long offset data, at which converted P-to-S arrivals are recorded.

Other tests performed without this two-step strategy, where both V_P and V_S parameters are reconstructed simultaneously from the beginning of the inversion process, failed and get stuck in a local minima.

FWI was performed for the same data as for the acoustic test: five frequencies were inverted successively (2, 3, 4, 5 and 6 Hz) with 3 damping factors applied in cascade for each frequency inversion ($\gamma = 2, 0.33, 0.1$). Starting models are shown in Figure 3. L-BFGS algorithm was used for optimization. We selected the diagonal of the Pseudo-Hessian (Shin et al., 2001) as

an initial guess for the L-BFGS iterations. Ten iterations were performed per damping factor, leading to 30 iterations per frequency inversion.

Results

Reconstructed V_P and V_S models and vertical logs at distances 3.5 and 8 *km* are displayed in Figures 7 and 8, respectively. The V_P model shows an accurate reconstruction of the main geological features, such as the anticlinal structure and the gas cloud in the sediments. The V_P model inferred from elastic inversion (Figure 7a) is close to that inferred from acoustic FWI (Figure 5), except in the deep part of the model (below 2.5 km), where elastic FWI provided improved reconstructions (compare Figures 6 and 8). The V_S model suffers from a deficit of short wavenumbers, especially in the deeper part where the starting model is less accurate. The very low velocities in the model endows the V_S imaging with a high resolution power, even at the low frequency of 2 Hz, that requires a very accurate starting model, a key issue in the prospect of real data processing. Amplitudes in the V_S model are not reconstructed as well as the V_P ones, and more iterations may be necessary to retrieve the correct amplitudes. The reconstructed models give, however, a useful information on the shallowest part of the target even for the V_S velocity model: these models would allow the identification and characterization of gas clouds, thanks to elastic properties variations.

CONCLUSION

This study presents an application of frequency-domain Full-Waveform Inversion of multi-components OBC data to the Valhall synthetic case study. The FWI algorithm is implemented through a two-loop scheme, over frequencies and time damping, to efficiently mitigate the non-linearities of the inversion. The quasi-Newton L-BFGS method is implemented for optimization.

The geological structure of the Valhall model makes the P arrivals dominant in the seismic wavefield, contrary to the S ones. On the one hand, P-wave velocity model can be successfully reconstructed by acoustic FWI, hence showing the relevance of the acoustic approximation for some marine case studies. On the other hand, elastic-parameters imaging is a difficult task, and complex multi-step strategies involving hierarchic inversions of data components and hierarchic reconstructions of different parameter classes must be designed to converge towards acceptable velocity models, if low frequencies and sufficiently-accurate starting models are not available. Future works will focus on the starting model building by Laplace-domain inversion (Shin and Cha, 2008) and PP-PS stereotomography (Alerini et al., 2002), before considering applications to real data.

ACKNOWLEDGMENTS

This study has been funded by the SEISCOPE consortium *http://seiscope.unice.fr*, sponsored by BP, CGG-VERITAS, EXXON-MOBIL, SHELL and TOTAL, and by ANR under project ANR-05-NT05-2-42427. Access to the high-performance computing facilities of MESOCENTRE SIGAMM (OCA) and IDRIS (CNRS) computer centers provided the required computer ressources. Many thanks go to J. Kommendal and L. Sirgue from BP for providing the elastic synthetic models of Valhall.

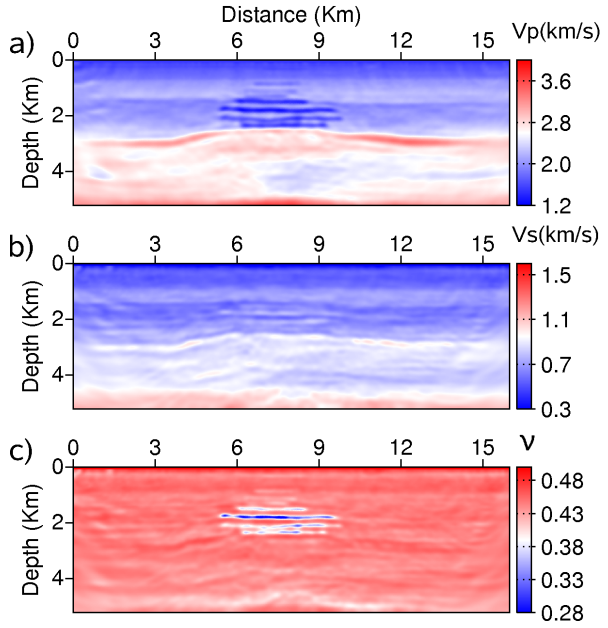

Figure 7: Reconstructed (a) V_P and (b) V_S models inferred from elastic FWI. (c) associated Poisson's ratio.

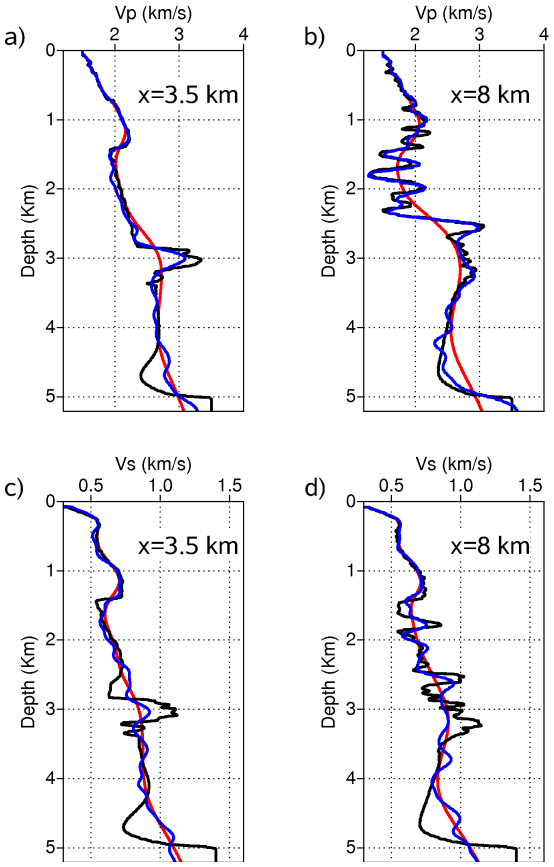

Figure 8: Vertical logs at distances a) 3.5 km and b) 8 km extracted from the FWI model of Figure 7. True, starting and FWI models are displayed in black, red and blue, respectively.

EDITED REFERENCES

Note: This reference list is a copy-edited version of the reference list submitted by the author. Reference lists for the 2009 SEG Technical Program Expanded Abstracts have been copy edited so that references provided with the online metadata for each paper will achieve a high degree of linking to cited sources that appear on the Web.

REFERENCES

Alerini, M., S. Le Bégat, G. Lambaré, and R. Baina, 2002, 2D PP- and PS-stereotomography for a multicomponent datset: 72nd Annual International Meeting, SEG, Expanded Abstracts, 838–841.

Amestoy, P. R., A. Guermouche, J. Y. L'Excellent, and S. Pralet, 2006, Hybrid scheduling for the parallel solution of linear systems: Parallel Computing, 32, 136–156.

Barnes, C. and M. Charara, 2008, Full-waveform inversion results when using acoustic approximation instead of elastic medium: 78th Annual International Meeting, SEG, Expanded Abstracts, 1895–1899.

Bleibinhaus, F., J. A. Hole, T. Ryberg, and G. S. Fuis, 2007, Structure of the California Coast Ranges and San Andreas Fault at SAFOD from seismic waveform inversion and reflection imaging: Journal of Geophysical Research, **112**, doi:10.1029/2006JB004611.

Brenders, A. J. and R. G. Pratt, 2007, Full waveform tomography for lithospheric imaging: Results from a blind test in a realistic crustal model: Geophysical Journal International, **168**, 133–151.

Brossier, R., S. Operto, and J. Virieux, 2009, 2D elastic frequency-domain full-waveform inversion for imaging complex onshore structures: 71th Conference & Exhibition, EAGE, Extended Abstracts, in press.

Brossier, R., J. Virieux, and S. Operto, 2008, Parsimonious finite-volume frequency-domain method for 2-D P-SV-wave modelling: Geophysical Journal International, **175**, 541–559.

Gelis, C., J. Virieux, and G. Grandjean, 2007, 2D elastic waveform inversion using Born and Rytov approximations in the frequency domain: Geophysical Journal International, **168**, 605–633.

Nocedal, J., 1980, Updating Quasi-Newton matrices with limited storage: Mathematics of Computation, **35**, 773–782.

Operto, S., J. Virieux, J. X. Dessa, and G. Pascal, 2006, Crustal imaging from multifold ocean bottom seismometers data by frequency-domain full-waveform tomography: Application to the eastern Nankai trough: Journal of Geophysical Research, **111**, doi:10.1029/2005JB003835.

Plessix, R.-E., 2006, A review of the adjoint-state method for computing the gradient of a functional with geophysical applications: Geophysical Journal International, **167**, 495–503.

Pratt, R. G., 1999, Seismic waveform inversion in the frequency domain, part I: Theory and verification in a physic scale model: Geophysical Journal International, **64**, 888–901.

Pratt, R. G., C. Shin, and G. J. Hicks, 1998, Gauss-Newton and full Newton methods in frequency-space seismic waveform inversion: Geophysical Journal International, **133**, 341–362.

Pratt, R. G., and M. H. Worthington, 1990, Inverse theory applied to multi-source cross-hole tomography. Part 1: Acoustic wave-equation method: Geophysical Prospecting, **38**, 287–310.

Ravaut, C., S. Operto, L. Improta, J. Virieux, A. Herrero, and P. dell'Aversana, 2004, Multi-scale imaging of complex structures from multi-fold wide-aperture seismic data by frequency-domain full-wavefield inversions: application to a thrust belt: Geophysical Journal International, **159**, 1032–1056.

Sears, T., S. Singh, and P. Barton, 2008, Elastic full waveform inversion of multi-component OBC seismic data: Geophysical Prospecting, **56**, 843–862.

Shi, Y., W. Zhao, and H. Cao, 2007, Nonlinear process control of wave-equation inversion and its application in the detection of gas: Geophysics, **72**, no. 1, R9–R18.

Shin, C. and Y. H. Cha, 2008, Waveform inversion in the Laplace domain: Geophysical Journal International, **173**, 922–931.

Shin, C., S. Jang, and D. J. Min, 2001, Improved amplitude preservation for prestack depth migration by inverse scattering theory: Geophysical Prospecting, 49, 592–606.

Sourbier, F., S. Operto, J. Virieux, P. Amestoy, and J.-Y. L'Excellent, 2009, FWT2D: A massively parallel program for frequency-domain full-waveform tomography of wide-aperture seismic data — Part 1: Algorithm: Computers & Geosciences, 35, 487–495.